X-ray dynamical diffraction analogues of the integer and fractional Talbot effects

Minas K. Balyan*

Faculty of Physics, Yerevan State University, Alex Manoogian 1, Yerevan 0025, Armenia. *Correspondence e-mail: mbalyan@ysu.am

The X-ray integer and fractional Talbot effect is studied under two-wave dynamical diffraction conditions in a perfect crystal, for the symmetrical Laue case of diffraction. The fractional dynamical diffraction Talbot effect is studied for the first time. A theory of the dynamical diffraction integer and fractional Talbot effect is given, introducing the dynamical diffraction comb function. An expression for the dynamical diffraction polarization-sensitive Talbot distance is established. At the rational multiple depths of the Talbot depth the wavefield amplitude for each dispersion branch is a coherent sum of the initial distributions, shifted by rational multiples of the object period and having its own phases. The simulated dynamical diffraction Talbot carpet for the Ronchi grating is presented.

1. Introduction

X-ray diffraction is a tool for investigating the structure of objects and crystals. A periodic object can be imaged using an X-ray monochromatic plane wave. The amplitude transmission coefficient of a periodic object is a periodic function of the coordinate along the axis, perpendicular to the propagation direction of the wave. The following question arises: what is the wavefield behaviour behind the object? This can be answered first in optics from the earlier work of Talbot (1836). Talbot experimentally showed that the field intensity periodically reproduces an initial periodic distribution. This period is called the Talbot distance and the effect is called the Talbot effect. Rayleigh (1881) gave a theoretical explanation of this effect. A formula for the Talbot distance, $z_T = 2D^2/\lambda$, where D is the period of the object and λ is the wavelength, was also given. Investigations of the Talbot effect in optics have continued to the present day (see, for example, Edgar, 1969; Guigay, 1971; Berry & Klein, 1996; Berry & Bodenschatz, 1999; Case et al., 2009; Kim et al., 2013).

We will concentrate our attention on the Talbot effect for X-rays ($\lambda \simeq 1$ Å). The first observation of the Talbot effect for X-rays was performed for a periodic phase object (Cloetens et al., 1997). The phase object self-image at the Talbot distance should have a uniform distribution. A simple formula for the amplitude was obtained at the distance $z_T/4$. The phase of the object can be determined via the intensity at the same distance. In the work of Momose et al. (2003), an X-ray Talbot interferometer was presented and investigated. The interferometer consisted of two separated gratings, placed at the Talbot distance from each other. By inclining the second grating around the optical axis, moiré fringes were obtained. An object placed in front of the first grating caused bending of the fringes. Momose et al. (2009) showed that the X-ray Talbot

Periodic object

X rays K_0^i θ^i

Crystal

RP h O x

Z

Diffracted beam   Transmitted beam
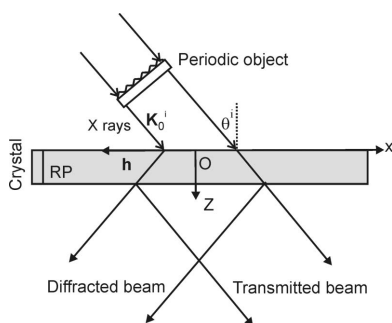
interferometer allows white synchrotron radiation to be used for high-speed imaging and tomography of soft materials and biological objects. Kim *et al.* (2010) demonstrated the Talbot effect for a broadband hard X-ray beam ($\Delta\lambda/\lambda \simeq 1$). The authors used a grating with sub-micrometer period. The X-ray Talbot effect has also been investigated for other types of objects (Kohn, 2016, 2018). The Talbot self-image of secondary periodically placed point sources, obtained in the focal plane of an array of compound parabolic lenses, was investigated by Kohn (2016). A theoretical investigation of the intensity distribution behind the photonic crystal inside the Talbot period was given by Kohn (2018). The plasmon analogue of the Talbot effect was theoretically analyzed by Dennis *et al.* (2007). Plasmons are electromagnetic waves excited on the surface of a metal. Excited interfering plasmon waves set up a Talbot carpet on the metal surface. The surface is planar, except for a periodic one-dimensional array of nanoholes. The plasmons are excited by means of a plane electromagnetic wave falling on the metal film surface.

In all cases described above, investigations of the Talbot effect were performed in free space, except for the work of Dennis *et al.* (2007), where the investigation was performed on the surface of a metal film.

In the work of Balyan (2019), for the first time the investigation of the X-ray Talbot effect was performed in a perfect crystal under the conditions of two-wave dynamical diffraction. The symmetrical Laue case was considered. Using the Green function formalism of dynamical diffraction an exact formula for the periodic object dynamical diffraction wavefield amplitude was obtained. The analysis, based on an approximation analogical to the paraxial approximation in optics, shows that in the diffracted field the analogue of the Talbot effect inside the crystal takes place. A formula for the dynamical diffraction Talbot distance is obtained, which, different to the case in free space, is polarization sensitive. The Talbot distance in the crystal is less than that in free space (2–50 m for a grating period of 10–50 µm) by a factor of 10^5 to 10^6. The simulated Talbot carpets inside the crystal were obtained for the first time.

The behaviour of the wavefield behind a periodic object in free space has interesting features not only at multiple distances of the Talbot distance (the integer Talbot effect) but also at distances which are odd multiples of half of the Talbot distance (also called the integer Talbot effect) and rational or irrational parts of the Talbot distance. At odd multiple distances of half of the Talbot distance, the initial distribution is repeated by a shift of half of the object period. At rational multiples of the Talbot distance (the fractional Talbot effect) the amplitude is a coherent sum of the initial distributions, shifted with respect to each other by a rational part of D and having its own phases (Guigay, 1971; Berry & Klein, 1996). At irrational multiple distances of the Talbot distance, the intensity is a fractal for gratings with sharp edges (Ronchi grating) (Berry & Klein, 1996). This effect is called the fractal Talbot effect in free space. Berry & Klein's (1996) investigation used the Dirac comb function (see the text) and the corresponding propagating comb waves.

The aim of this paper is to investigate the dynamical diffraction integer and fractional Talbot effects introducing the comb function for the dynamical diffraction case in the diffracted beam. The latter is the diffracted wave, when a Dirac comb wave falls on the surface of the crystal. Both modes of the dispersion surface inside the crystal forms its own set of Talbot images, which interfere with each other. Thus, the dynamical diffraction integer and fractional Talbot effects are accompanied by Pendellösung oscillations. The contribution of each branch of the dispersion surface in the fractional and integer Talbot effect will be analyzed. The dynamical diffraction reflection coefficients of spatial harmonics of an initial periodic distribution give the Bragg filtration of higher-order spatial harmonics in the diffracted beam inside the crystal. The absorption and polarization also affect the dynamical diffraction integer and fractional Talbot effects. As a result of the influence of the dynamical diffraction reflection coefficients and absorption, even for a phase object, at multiple Talbot distances the intensity is not uniform (contrary to the case in free space). The fractional dynamical diffraction Talbot effect will be compared with the fractional Talbot effect in free space. The symmetrical Laue geometry diffraction in the case of an incident plane monochromatic wave will be considered. Examples for a cosine-like grating and for a Ronchi grating are presented.

2. Basic formulas

The scheme for studying the Talbot effect for X-ray symmetrical Laue case dynamical diffraction in ideal crystals is shown in Fig. 1. An X-ray monochromatic beam with a wavevector $\mathbf{K}_0^i$ (wavelength λ) and unit amplitude, passing through an object with a periodic complex amplitude transmission coefficient $T(x) = T(x + D)$, falls on the entrance surface of a perfect crystal at an angle θ^i relative to the atomic reflecting planes RP, which are perpendicular to the entrance surface of the crystal. The angle θ^i is close to the Bragg angle θ for the diffraction vector $\mathbf{h}$, and transmitted and diffracted waves are formed in the crystal.
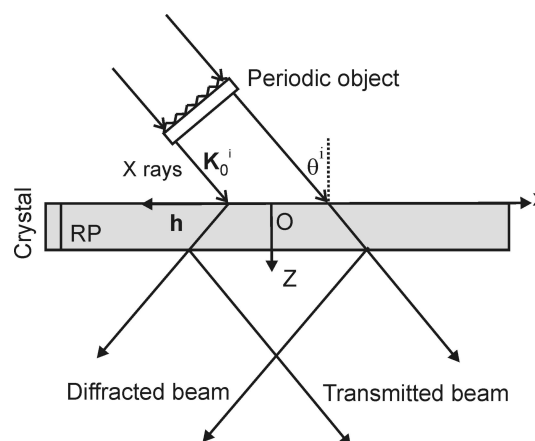

Figure 1
Scheme of the X-ray dynamical diffraction Talbot effect. On the path of the incident beam an object with a periodic complex amplitude transmission coefficient is placed.

The transmission coefficient can be expanded in the Fourier series,

$$T(x) = \sum_{n=-\infty}^{+\infty} A_n \exp\left(2\pi in \frac{x}{D}\right), \tag{1}$$

$$A_n = \frac{1}{D} \int_{-D/2}^{D/2} T(x) \exp\left(-2\pi in \frac{x}{D}\right) dx. \tag{2}$$

The Ox axis of the selected coordinate system is antiparallel to the diffraction vector $\mathbf{h}$. The Oz axis is perpendicular to the entrance surface, and the Oy axis is perpendicular to the xz diffraction plane. The electrical field for the incident wave has the form $\mathbf{E}_0^i = (E_{0\sigma}^i \mathbf{e}_\sigma + E_{0\pi}^i \mathbf{e}_{0\pi}) \exp(i\mathbf{K}_0^i \mathbf{r})$. The electrical fields for the transmitted and diffracted waves inside the crystal are presented as $\mathbf{E}_0 = (E_{0\sigma} \mathbf{e}_\sigma + E_{0\pi} \mathbf{e}_{0\pi}) \exp(i\mathbf{K}_0 \mathbf{r})$ and $\mathbf{E}_h = (E_{h\sigma} \mathbf{e}_\sigma + E_{h\pi} \mathbf{e}_{h\pi}) \exp(i\mathbf{K}_h \mathbf{r})$. Here are introduced the polarization unit vectors $\mathbf{e}_\sigma$ (parallel to the axis Oy, i.e. perpendicular to the diffraction plane xz), $\mathbf{e}_{0\pi} = [\mathbf{s}_0 \mathbf{e}_\sigma]$ (polarization vector for the incident and transmitted waves, lying in the diffraction plane) and the polarization vector $\mathbf{e}_{h\pi} = [\mathbf{s}_h \mathbf{e}_\sigma]$ for the diffracted wave. $\mathbf{e}_{0\pi}$ and $\mathbf{e}_{h\pi}$ are perpendicular to the wavevectors $\mathbf{K}_0$ and $\mathbf{K}_h = \mathbf{K}_0 + \mathbf{h}$, respectively; $\mathbf{s}_0$ and $\mathbf{s}_h$ are the unit vectors along the propagation directions of the transmitting and diffracted waves, respectively. The wavevectors are chosen so that they satisfy the exact Bragg condition $\mathbf{K}_0^2 = \mathbf{K}_h^2 = k^2 = (2\pi/\lambda)^2$. The amplitudes for each polarization state, as is well known, satisfy Takagi's equations (Takagi, 1962, 1969),

$$\frac{2i}{k} \frac{\partial E_0}{\partial s_0} + \chi_0 E_0 + C\chi_{\bar{h}} E_h = 0,$$
$$\frac{2i}{k} \frac{\partial E_h}{\partial s_h} + \chi_0 E_h + C\chi_h E_0 = 0. \tag{2a}$$

Here, $\chi_0 = \chi_{0r} + i\chi_{0i}$, $\chi_h = \chi_{hr} + i\chi_{hi}$ and $\chi_{\bar{h}} = \chi_{\bar{h}r} + i\chi_{\bar{h}i}$ are the Fourier coefficients of the crystal susceptibility for the diffraction vectors 0, $\mathbf{h}$ and $\bar{\mathbf{h}}$, respectively (the indices 'r' and 'i' refer to the real and imaginary parts of the susceptibility of the crystal, respectively), C is the polarization factor and equals unity for σ-polarization and $\cos 2\theta$ for π-polarization.

We will find the amplitude of the diffracted wave in the crystal for the case of a plane monochromatic incident wave. According to the dynamical diffraction theory the amplitude of the diffracted wave inside the crystal can be presented as a convolution of the incident wave amplitude and the corresponding Green function along the entrance surface of the crystal (Takagi, 1969; Authier, 2001; Pinsker, 1982). In this way, also using (1), for the amplitude of a σ-polarized diffracted wave, we obtain

$$E_h(x, z) = \sum_{n=-\infty}^{+\infty} A_n \int_{x-z\tan\theta}^{x+z\tan\theta} G(x-x', z) \exp\left(2\pi in \frac{x'}{D}\right)$$
$$\times \exp(ikx' \cos\theta \, \Delta\theta) \, dx', \tag{3}$$

where the Green function

$$G(x, z) = \frac{ik\chi_h}{4\sin\theta} \exp\left(ik\frac{\chi_0 z}{2\cos\theta}\right)$$
$$\times J_0\left[\frac{\pi c \tan\theta}{\Lambda}\left(z^2 \tan^2\theta - x^2\right)^{1/2}\right]$$
$$\times H(z\tan\theta - |x|), \tag{4}$$

$\Delta\theta = \theta^i - \theta$ is the deviation from the Bragg exact angle, $\Lambda = \lambda \cos\theta/(\chi_h \chi_{\bar{h}})^{1/2}$ ($\Lambda_r = \text{Re}\,\Lambda$ is the extinction length), J_0 is the zero-order Bessel function and H is the Heaviside step function. Without loss of generality, we consider the case of a σ-polarized wave. In the case of π-polarization, in the final formulas, χ_h and $\chi_{\bar{h}}$ must be replaced by $\chi_h \cos 2\theta$ and $\chi_{\bar{h}} \cos 2\theta$, respectively. According to Balyan (2019), the solution (3) can be presented as

$$E_h(x, z) = i\left(\frac{\chi_h}{\chi_{\bar{h}}}\right)^{1/2} \exp\left(ik\frac{\chi_0 z}{2\cos\theta}\right) \exp(ikx \cos\theta \, \Delta\theta)$$
$$\times \sum_{n=-\infty}^{+\infty} A_n \exp\left(2\pi in \frac{x}{D}\right) \frac{\sin \pi(z/\Lambda) \Omega_n}{\Omega_n}, \tag{5}$$

where

$$\Omega_n = \left(1 + p_n^2\right)^{1/2}, \tag{6}$$

$$p_n = \frac{\Delta_n \theta}{\left(\chi_h \chi_{\bar{h}}\right)^{1/2}} \sin 2\theta \tag{7}$$

and

$$\Delta_n \theta = \Delta\theta + \frac{2\pi n}{kD \cos\theta}. \tag{8}$$

Following the method given by Berry & Klein (1996), we represent the solution using a comb wave. Such a wave corresponds to the situation when the amplitude of the wave, incident on the crystal, is the Dirac comb,

$$E_0^i = \sum_{n=-\infty}^{\infty} \delta(x - nD) = \frac{1}{D} \sum_{n=-\infty}^{\infty} \exp\left(2\pi in \frac{x}{D}\right). \tag{9}$$

In this case

$$A_n = 1/D. \tag{10}$$

Formula (9) is called the Poisson formula. Thus, from (5) and (10), for the case of the incident Dirac comb wave, the solution is obtained in the form of a comb wave,

$$E_{h\,\text{comb}}(x, z) = i\left(\frac{\chi_h}{\chi_{\bar{h}}}\right)^{1/2} \exp\left(ik\frac{\chi_0 z}{2\cos\theta}\right) \exp(ikx \cos\theta \, \Delta\theta) \frac{1}{D}$$
$$\times \sum_{n=-\infty}^{+\infty} \exp\left(2\pi in \frac{x}{D}\right) \frac{\sin \pi(z/\Lambda) \Omega_n}{\Omega_n}. \tag{11}$$

Substituting (2) into (5), the solution in the general case of a falling periodic function, as is easily seen, is represented in the form of the convolution

$$E_h(x, z) = \int_{-D/2}^{D/2} T(x') E_{h\,\text{comb}}(x - x', z) \, dx'. \tag{12}$$

Thus, the study of dynamical diffraction of a periodic incident field leads to the study of the properties of a comb wave.

For analytical consideration it is necessary to use some approximations. Compared with the cases of effects in free space, in the case of dynamical diffraction in an ideal crystal, some difficulties arise. In (11), due to absorption, Λ, p_n and, therefore, Ω_n are complex, the Fourier coefficients of the comb wave are multiplied by the reflection coefficient $1/\Omega_n$ and, moreover, due to the existence of two sheets of the dispersion surface, the comb wave is a coherent superposition of two comb waves corresponding to the two sheets of the dispersion surface. These difficulties can be overcome by using some approximations. In most cases of dynamical diffraction the frequency of the incident radiation is greater than the resonant frequencies of the atoms of the crystal. Therefore, $\chi_{0i} \ll |\chi_{0r}|$ and $|\chi_{hi}| \ll |\chi_{hr}|$. It is easy to see that, with the accuracy of the terms $\chi_{hi}/|\chi_{hr}|$ inclusive (Balyan, 2019), the following approximation is valid,

$$\pi \frac{z}{\Lambda} \Omega_n \simeq \pi \frac{z}{\Lambda_r} \Omega_{nr} - i \frac{kz\chi_{hi}}{2\cos\theta\,\Omega_{nr}}, \tag{13}$$

where

$$\Omega_{nr} = \mathrm{Re}\,\Omega_n = \left(1 + p_{nr}^2\right)^{1/2} \tag{14}$$

and

$$p_{nr} = \mathrm{Re}\,p_n = \frac{\sin 2\theta\,\Delta_n\theta}{|\chi_{hr}|}. \tag{15}$$

Note that in the framework of this approximation, $\Lambda_r = \mathrm{Re}\,\Lambda = \lambda\cos\theta/|\chi_{hr}|$. The expression (13), without loss of generality, is written for centrosymmetric crystals, i.e. it is suggested that $\chi_h = \chi_{\bar{h}}$, $\chi_{hr} < 0$ and $\chi_{hi} > 0$. Let us replace the Fourier coefficients A_n by

$$A_{n\pm}(z) = \frac{A_n}{\Omega_{nr}}\exp\left(-\frac{\mu_{dn\pm}z}{2\cos\theta}\right), \tag{16}$$

where

$$\mu_{dn\pm} = \mu\left(1 \mp \frac{\chi_{hi}}{\chi_{0i}\,\Omega_{nr}}\right) \tag{17}$$

are the diffraction absorption coefficients for both branches of the dispersion surface, and

$$\mu = k\chi_{0i} \tag{18}$$

is the linear absorption coefficient of the crystal. Let us also introduce new functions, periodic in the variable x,

$$T_\pm(x, z) = \sum_{n=-\infty}^{\infty} A_{n\pm}(z)\exp\left(\frac{2\pi i n x}{D}\right). \tag{19}$$

Then, instead of (12), one can write

$$E_h(x, z) = \int_{-D/2}^{D/2} \left[T_+(x', z)\,E_{h\,\mathrm{comb}+}(x - x', z) - T_-(x', z)\right.$$
$$\left. \times E_{h\,\mathrm{comb}-}(x - x', z)\right]\mathrm{d}x'. \tag{20}$$

New comb waves have also been introduced here,

$$E_{h\,\mathrm{comb}\pm}(x, z) = \exp\left(ik\frac{\chi_{0r}z}{2\cos\theta}\right)\exp(ikx\cos\theta\,\Delta\theta)\frac{1}{2D}$$
$$\times \sum_{n=-\infty}^{+\infty}\exp\left(2\pi i n\frac{x}{D}\right)\exp\left(\pm i\pi\frac{z}{\Lambda_r}\Omega_{nr}\right). \tag{21}$$

Further analysis is carried out for the case $\Delta\theta = 0$, which is the analogue of the perpendicular falling of the wave onto the plane of a periodic object, in optics, i.e. for the case of the Talbot effect (Case et al., 2009). As can be seen from (16), the new introduced Fourier coefficients faster than the originals, with increasing order numbers, tend to zero. As a result, in (19) the main contribution comes from harmonics, for which $p_{nr}^2 < 1$. Therefore, in (21), one can use the approximation

$$\Omega_{nr} \simeq 1 + \frac{p_{nr}^2}{2}, \tag{22}$$

which is equivalent to the paraxial approximation in optics. This approximation here is also called paraxial. The condition $p_{nr}^2 < 1$ of the paraxial approximation, according to definition (15), is equivalent to the condition $n^2 < (D/2\Lambda_r \tan\theta)^2$. A more accurate analysis, based on the evaluation of the neglected terms (Balyan, 2019), shows that it is sufficient to require the condition

$$n^2 < \left(\frac{D}{\Lambda_r \tan\theta}\right)^2. \tag{23}$$

After substituting (22) into expression (21), one can write

$$E_{h\,\mathrm{comb}\pm}(x, z) \simeq \frac{1}{2}\exp\left(ik\frac{\chi_{0r}z}{2\cos\theta}\right)\exp\left(\pm i\pi\frac{z}{\Lambda_r}\right)E_{hp\pm}(x, z), \tag{24}$$

where

$$E_{hp\pm}(x, z) = \frac{1}{D}\sum_{n=-\infty}^{+\infty}\exp\left(2\pi i n\frac{x}{D}\right)\exp\left(\pm i\pi\frac{z}{\Lambda_r}\frac{p_{nr}^2}{2}\right). \tag{25}$$

In the paraxial approximation, from (20), we have

$$E_h(x, z) = \frac{1}{2}\exp\left(ik\frac{\chi_{0r}z}{2\cos\theta}\right)\int_{-D/2}^{D/2}\left[T_+(x', z)\exp\left(i\pi\frac{z}{\Lambda_r}\right)\right.$$
$$\times E_{hp+}(x - x', z) - T_-(x', z)\exp\left(-i\pi\frac{z}{\Lambda_r}\right)$$
$$\left.\times E_{hp-}(x - x', z)\right]\mathrm{d}x'. \tag{26}$$

In (25), for further analysis, it is convenient to introduce the depth,

$$z_{\mathrm{Td}} = \frac{D^2}{\Lambda_r \tan^2\theta}, \tag{27}$$

and write

$$E_{hp\pm}(x, z) = \frac{1}{D}\sum_{n=-\infty}^{+\infty}\exp\left(2i\pi n\frac{x}{D}\right)\exp\left(\pm 2i\pi n^2\frac{z}{z_{\mathrm{Td}}}\right). \tag{28}$$

It is convenient, also, to present (26) in the form

$$E_h(x, z) = \frac{1}{2}\exp\left(ik\frac{\chi_{0r}z}{2\cos\theta}\right) \tag{29}$$
$$\times \left[\exp\left(i\pi\frac{z}{\Lambda_r}\right)E_{h+} - \exp\left(-i\pi\frac{z}{\Lambda_r}\right)E_{h-}\right],$$

where

$$E_{h\pm}(x, z) = \int_{-D/2}^{D/2} T_\pm(x', z)\, E_{hp\pm}(x - x', z)\, dx'. \tag{30}$$

Note that

$$E_{hp+}(x, z) = E_{hp-}^*(x, z), \tag{31}$$

where * denotes the complex conjugate. The expression for $E_{hp-}(x, z)$ coincides with the corresponding expression in free space (Berry & Klein, 1996); therefore, as in Berry & Klein (1996), this function will be called the paraxial propagator. Thus, the features of a dynamically diffracted wavefield in a crystal, as in free space, are based on the properties of the same paraxial propagator.

3. Integer dynamical diffraction Talbot effect

The integral dynamical diffraction Talbot effect has already been studied by Balyan (2019). We will analyze this effect here based on formulas (28)–(31). Note that, according to (28), the function $E_{hp-}(x, z)$ is periodic in x, with period D. In addition, this function is periodic in the variable z, with a period z_{Td}. The initial distribution of this function, the Dirac comb function (9), is repeated at depths $z = lz_{Td}$ ($l = 0, 1, 2, \ldots$). By analogy with the case in free space (Berry & Klein, 1996), the depth z_{Td} we call the dynamical diffraction Talbot depth (Balyan, 2019). At depths $z = (2l + 1)z_{Td}/2$ ($l = 0, 1, 2, \ldots$), as can be seen from (28), the initial distribution (9) is repeated with a shift $D/2$ along the Ox axis. It can be said that at depths $z = lz_{Td}/2$ the initial distribution of the Dirac comb function is repeated for even l, and for odd l it is repeated with a shift of $D/2$ along the Ox axis. In this sense, there is a dynamical diffraction integer Talbot effect for the paraxial propagator. In free space, the role of z_{Td} is played by the Talbot distance, defined as $z_T = 2D^2/\lambda$ (Berry & Klein, 1996). This property, in free space, of the paraxial propagator implies the same property of repetition of the initial distribution $T(x)$ also for the propagating wave. This follows from the analogue of relation (30) in free space (Berry & Klein, 1996). This effect is called the integer Talbot effect in free space. We should investigate the existence of the same effect in the case of dynamical diffraction, based on relations (28)–(31). As can be seen from (16), the Fourier spectrum of the initial distribution changes due to Bragg diffraction. In addition, the Fourier coefficients, due to absorption, become monotonically decreasing functions of z. But the diffracted wave is still periodic in x with period D. Thus, since the paraxial propagator in the crystal remains a periodic function of z with period z_{Td}, from (30) it follows that the amplitudes $E_{h\pm}(x, z)$ [equations (29) and (30)] will be quasiperiodic in z with period z_{Td}. At depths $z = lz_{Td}$ ($l = 1, 2, \ldots$), $E_{h\pm}(x, z)$ will repeat the initial

distributions $T_\pm(x, z)$, i.e. they will repeat the initial distribution approximately. It can also be argued that at depths $z = (2l + 1)z_{Td}/2$ ($l = 0, 1, 2, \ldots$) the diffracted wave will approximately repeat the initial distribution with the shift $D/2$ along the Ox axis. This is the integer Talbot effect in the case of dynamical diffraction. More specifically, from (30) it follows that, with $z = lz_{Td}$ ($l = 1, 2, \ldots$),

$$E_{h\pm}(x, z) = \pm T_\pm(x, z). \tag{32}$$

If $z = (2l + 1)z_{Td}/2$ ($l = 0, 1, 2, \ldots$), again, from (30), it follows

$$E_{h\pm}(x, z) = \pm T_\pm(x + D/2, z). \tag{33}$$

From (29), (32) and (33) at $z = lz_{Td}$ ($l = 1, 2, \ldots$), it follows

$$E_h(x, z) = \frac{1}{2}\exp\left(ik\frac{\chi_{0r}z}{2\cos\theta}\right) \tag{34}$$
$$\times \left[\exp\left(i\pi\frac{z}{\Lambda_r}\right)T_+(x, z) - \exp\left(-i\pi\frac{z}{\Lambda_r}\right)T_-(x, z)\right],$$

and at $z = (2l + 1)z_{Td}/2$ ($l = 0, 1, 2, \ldots$)

$$E_h(x, z) = \frac{1}{2}\exp\left(ik\frac{\chi_{0r}z}{2\cos\theta}\right)\left[\exp\left(i\pi\frac{z}{\Lambda_r}\right)T_+(x - D/2, z)\right.$$
$$\left. - \exp\left(-i\pi\frac{z}{\Lambda_r}\right)T_-(x - D/2, z)\right]. \tag{35}$$

According to (34) and (35), for the intensity $I_h(x, z) = |E_h(x, z)|^2$ we find

$$I_h(x, z) = \frac{1}{4}\left[T_+^2(x, z) + T_-^2(x, z)\right.$$
$$\left. - 2T_+(x, z)\, T_-(x, z)\cos\left(2\pi\frac{z}{\Lambda_r}\right)\right],$$
$$\text{for} \quad z = lz_{Td} \ (l = 1, 2, \ldots), \tag{36}$$

$$I_h(x, z) = \frac{1}{4}\left[T_+^2(x - D/2, z) + T_-^2(x - D/2, z)\right.$$
$$\left. - 2T_+(x - D/2, z)\, T_-(x - D/2, z)\cos\left(2\pi\frac{z}{\Lambda_r}\right)\right],$$
$$\text{for} \quad z = (2l + 1)z_{Td}/2 \ (l = 0, 1, 2, \ldots).$$

Note that according to condition (23) and definition (27), the condition (23) can be written as

$$z_{Td} > \Lambda_r. \tag{37}$$

It follows from (36) that at depths $z = lz_{Td}$ ($l = 1, 2, \ldots$) and $z = (2l + 1)z_{Td}/2$ ($l = 0, 1, 2, \ldots$), in the case of the dynamical diffraction Talbot effect, because of the presence of two branches of the dispersion surface, the reconstructed distributions $T_\pm(x, z)$ interfere coherently. To further analyze the resulting expression (36), we first consider the case without a periodic object. Then $A_0 = 1$ and $A_n = 0$ for $n \neq 0$, and from (36) it follows that pendulum oscillations, i.e. interference fringes over the crystal depth, with a period Λ_r are obtained. In the case of a periodic object, at the same time we have

depth oscillations with periods z_{Td} and $z_{Td}/2$ and pendulum oscillations. Consequently, the maxima of the periodic distribution over z_{Td} will be cut by several lines of the pendulum oscillations. At the depths $\mu z \gg 1$, the highly absorbing branch with the '−' index does not make a noticeable contribution to the intensity. At such depths, only a weakly absorbing branch with the '+' index remains. Therefore, the pendulum oscillations vanish and oscillations in z_{Td} and $z_{Td}/2$ only of the weakly absorbed mode remain. Note that an important consequence follows from the expression (19). If the object is a phase object, then in free space its self-image will have a homogeneous intensity distribution (Cloetens *et al.*, 1997). Inside the crystal, the self-image intensity distribution is not homogeneous and will have a contrast.

4. Fractional dynamical diffraction Talbot effect

Investigations of the Talbot effect in free space show that at distances $z = (l + q/r)z_{Td}$, where l, r and q are non-negative integers, $q < r$ and r and q are mutually prime numbers, the features of the Talbot images can also be revealed analytically (Guigay, 1971; Berry & Klein, 1996; Case *et al.*, 2009). We should investigate these images in the case of dynamical diffraction. Following the work of Case *et al.* (2009), we substitute the value $z = (l + q/r)z_{Td}$ into (28). Then we obtain

$$E_{hp-}(x, z) = \frac{1}{D} \sum_{n=-\infty}^{+\infty} \exp\left(2i\pi n \frac{x}{D}\right) \exp\left(-2i\pi n^2 \frac{q}{r}\right). \quad (38)$$

The term $\exp(-2i\pi n^2 q/r)$ is periodic in n with period r. Therefore, this term can be expanded into a discrete Fourier series,

$$\exp\left(-2i\pi n^2 \frac{q}{r}\right) = \sum_{m=0}^{r-1} a_m \exp\left(-2i\pi m \frac{n}{r}\right). \quad (39)$$

The coefficients a_m are determined using the relations

$$\sum_{n=0}^{r-1} \exp\left(-2i\pi m \frac{n}{r}\right) \exp\left(-2i\pi m' \frac{n}{r}\right) = r\delta_{mm'}. \quad (40)$$

Thus, from (39) and (40), we have

$$a_m = \frac{1}{r} \sum_{n=0}^{r-1} \exp\left[-2i\pi(n^2 - mn)\frac{q}{r}\right]. \quad (41)$$

Substituting (39) into (38), we find

$$E_{hp-}(x, z) = \frac{1}{D} \sum_{m=0}^{r-1} a_m \sum_{n=-\infty}^{+\infty} \exp\left[2i\pi n \frac{(x - mD/r)}{D}\right]. \quad (42)$$

According to the formula (9), from (42) we have

$$E_{hp-}(x, z) = \sum_{m=0}^{r-1} a_m \delta(x - mD/r - nD), \quad (43)$$

and according to (21)

$$E_{hp+}(x, z) = \sum_{m=0}^{r-1} a_m^* \delta(x - mD/r - nD). \quad (44)$$

Substituting (43) and (44) into (29), and performing integration, for the amplitude at the depth $z = (l + q/r)z_{Td}$, we find the expression

$$E_h(x, z) = \frac{1}{2} \exp\left(ik\frac{\chi_{0r}z}{2\cos\theta}\right)$$
$$\times \left[\exp\left(i\pi\frac{z}{\Lambda_r}\right) \sum_{m=0}^{r-1} a_m^* T_+(x - mD/r, z) \right.$$
$$\left. - \exp\left(-i\pi\frac{z}{\Lambda_r}\right) \sum_{m=0}^{r-1} a_m T_-(x - mD/r, z) \right]. \quad (45)$$

Thus, the Talbot fractional effect is a field consisting of a coherent superposition of r displaced relative to the other terms of the initial distribution, multiplied by the corresponding coefficient a_m. In the case of dynamical diffraction each branch of the dispersion surface has its own collection of initial distributions and these two sets also interfere with each other. In the case of dynamical diffraction, the Fourier coefficients of the initial distribution are changed due to Bragg filtering of the harmonics, and also depend on z due to absorption.

It follows from the derivation that (45) can also be used for $q = 1$ and $r = 1$. In this case, from (41), it follows that $a_0 = 1$. Then (45) goes into (34), *i.e.* we obtain the integer Talbot effect at the depths $z = lz_{Td}$ ($l = 1, 2, \dots$). In the case of $q = 1$ and $r = 2$, from (41), we have $a_0 = 0$ and $a_1 = 1$. Therefore, (45) and (35) coincide, *i.e.* the Talbot integer effect for the depths $z = (2l + 1)z_{Td}/2$ ($l = 0, 1, 2, \dots$) is obtained. In the general case, the coefficients a_m are the Gauss sum (Berry & Klein, 1996), known in classical number theory. Here we consider a few special cases.

4.1. Case I: $z = z_{Td}/4$, *i.e.* $q = 1$, $r = 4$

In this case, according to (41), $a_0 = (1/\sqrt{2})\exp(-i\pi/4)$, $a_1 = 0$, $a_2 = (1/\sqrt{2})\exp(i\pi/4)$, $a_3 = 0$. Substituting these values into (45), we find

$$E_h(x, z) = \frac{1}{2\sqrt{2}} \exp\left(ik\frac{\chi_{0r}z}{2\cos\theta}\right)\left\{ \exp\left(i\pi\frac{z}{\Lambda_r}\right) \right.$$
$$\times \left[\exp(i\pi/4)\, T_+(x, z) \right.$$
$$\left. + \exp(-i\pi/4)\, T_+(x - D/2, z) \right]$$
$$- \exp\left(-i\pi\frac{z}{\Lambda_r}\right)\left[\exp(-i\pi/4)\, T_-(x, z) \right.$$
$$\left.\left. + \exp(i\pi/4)\, T_-(x - D/2, z) \right] \right\}. \quad (46)$$

4.2. Case II: $z = z_{Td}/8$, *i.e.* $q = 1$, $r = 8$

In this case, from (41) we have $a_0 = \exp(-i\pi/4)/2$, $a_1 = 0$, $a_2 = 1/2$, $a_3 = 0$, $a_4 = -\exp(-i\pi/4)/2$, $a_5 = 0$, $a_6 = 1/2$, $a_7 = 0$. Accordingly, substituting these values into (45) for the amplitude of the diffracted wave, we find

$$E_h(x, z) = \frac{1}{4} \exp\left(ik \frac{\chi_{0r} z}{2 \cos \theta}\right)$$

$$\times \left(\exp\left(i\pi \frac{z}{\Lambda_r}\right) \left\{ \exp(i\pi/4) \left[T_+(x, z) + T_+(x - D/2, z)\right] \right. \right.$$

$$\left. + T_+(x - D/4, z) + T_+(x - 3D/4, z) \right\}$$

$$- \exp\left(-i\pi \frac{z}{\Lambda_r}\right) \left\{ \exp(-i\pi/4) \left[T_-(x, z) + T_-(x - D/2, z)\right] \right.$$

$$\left. \left. + T_-(x - D/4, z) + T_-(x - 3D/4, z) \right\} \right). \tag{47}$$

4.3. Case III: $z = 3z_{Td}/4$, i.e. $q = 3$, $r = 4$

From formula (41) we obtain $a_0 = (1 + i)/2$, $a_1 = a_3 = 0$, $a_2 = (1 - i)/2$. Substituting these values into (45), for the amplitude we obtain

$$E_h(x, z) = \frac{1}{2\sqrt{2}} \exp\left(ik \frac{\chi_{0r} z}{2 \cos \theta}\right)$$

$$\times \left\{ \exp\left(i\pi \frac{z}{\Lambda_r}\right) \left[\exp(-i\pi/4) T_+(x, z) \right. \right.$$

$$\left. + \exp(i\pi/4) T_+(x - D/2, z)\right]$$

$$- \exp\left(-i\pi \frac{z}{\Lambda_r}\right) \left[\exp(i\pi/4) T_-(x, z) \right.$$

$$\left. \left. + \exp(-i\pi/4) T_-(x - D/2, z)\right] \right\}. \tag{48}$$

Comparing expressions (46)–(48) with the corresponding expressions in free space (Guigay, 1971; Cloetens *et al.*, 1997), one can notice that the terms for the branch $\exp(-i\pi z/\Lambda_r)$ coincide with the expressions in free space. However, in the crystal there is also an image from another branch of the dispersion surface. The fractional Talbot effect in a crystal is accompanied by the interference of images of two branches of the dispersion surface, *i.e.* accompanied by pendulum oscillations.

5. Examples of dynamic diffraction integer and fractional Talbot effects

In order to verify the conclusions of the approximate, analytical consideration, we can numerically simulate images inside a crystal, based on the exact formula (5) or use the exact formulas (11) and (12).

In both cases, bearing in mind that $|1/\Omega_n|$ monotonously decreases with increasing $|n|$, in the case of an object with an infinite set of harmonics, one can keep a finite number of terms both in (5) and (11). With an increase in $|n|$, the Fourier coefficients also decrease due to absorption, see (16).

To illustrate the above-obtained results, as an example, consider the reflection of Si (220) for Mo $K\alpha$ radiation ($\lambda = 0.71$ Å, $\theta = 10.63°$), σ-polarization. For silicon, $\chi_{0r} = -3.162 \times 10^{-6}$, $\chi_{0i} = 0.165 \times 10^{-7}$, $\chi_{hr} = \chi_{\bar{h}r} = -1.901 \times 10^{-6}$, $\chi_{hi} = \chi_{\bar{h}i} = 0.159 \times 10^{-7}$ (Pinsker, 1982). Accordingly, we have, $\Lambda_r =$

36.6 μm and $\Lambda_r \tan \theta = 6.9$ μm. The deviation from the exact Bragg condition $\Delta\theta = 0$.

5.1. Cosine-like grating

As a periodic object, we take an object with a limited Fourier spectrum: a cosine-like grating. In this case,

$$T(x) = \frac{1 + \cos(2\pi x/D)}{2}, \tag{49}$$

$A_0 = 0.5$, $A_{\pm 1} = 0.25$ and $A_n = 0$ for $|n| > 1$. Fig. 2(a) depicts the initial distribution $T^2(x)$.
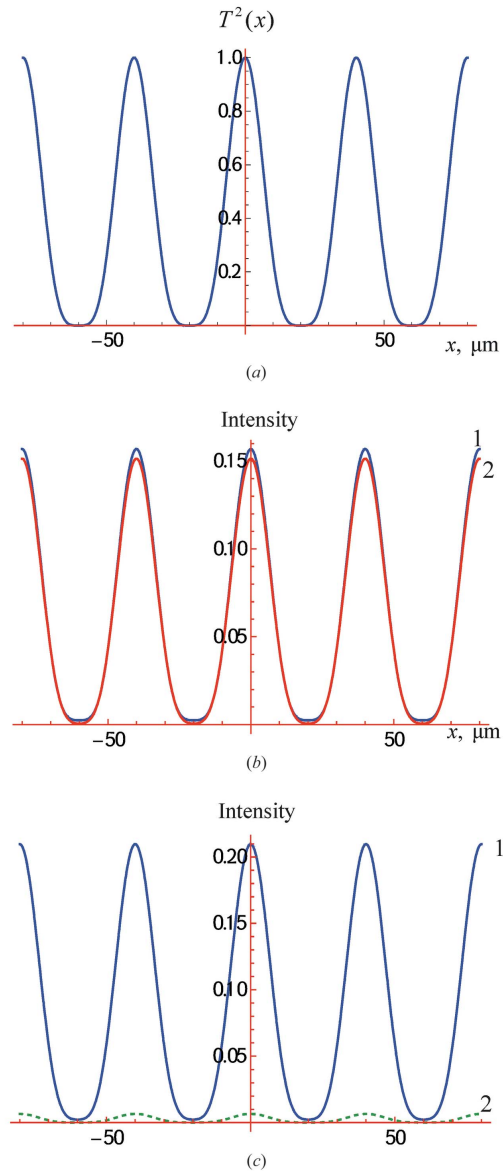

Figure 2
The integer dynamical diffraction Talbot effect at the depth z_{Td} for a cosine-like grating. (a) The intensity of the initial distribution $T^2(x)$. (b) The intensity inside the crystal, according to the exact formula (5) (curve 1, blue) and according to the approximate formula (36) (curve 2, red). (c) Comparison of the intensities of the weakly absorbing (curve 1, blue) and strongly absorbing modes (curve 2, green), calculated by the exact formula (5).

In the case of $D = 40\ \mu m$, we have $z_{Td} = 1.2$ mm and $D/(\Lambda_r \tan\theta) = 5.8$. It follows from the last relation that the condition (23) of the paraxial approximation is sufficiently well satisfied. Note that in free space, according to the formula for the Talbot distance $z_T = 2D^2/\lambda$ (Berry & Klein, 1996; Cloetens *et al.*, 1997), the Talbot distance $z_T = 45.2$ m. We will compare the intensity distributions at the depth z_T for the integer Talbot effect, using the approximate expression (36) and comparing with the exact expression (5). Comparison of the intensity distributions for the fractional Talbot effect at the depth $z_T/4$ is carried out on the basis of the approximate expression (46) and the exact expression (5).

Fig. 2(*b*) shows the intensity distribution at the depth z_T based on the exact formula (5) and the approximate expression (36). As can be seen from this figure, the intensity of the approximate expression agrees well with the intensity calculated by the exact formula. This result is a direct consequence of the good fulfilment of the condition of the paraxial approximation (23). Both intensities, with an accuracy of accounting for the Bragg dependence of harmonics, absorption and the interference effect of two branches (the pendulum effect), coincide with the initial distribution. In order to identify the effects of the pendulum effect on the resulting distribution, Fig. 2(*b*) shows the intensities of both branches separately, as well as the full distribution, calculated by the exact formula (5). As can be seen from this figure, both branches reproduce the initial distribution, the difference being that the strongly absorbing mode has a much lower intensity. According to (17), for these branches, the dynamic absorption is determined by the values $\mu_{d0+}z_{Td} = 0.07$ and $\mu_{d0-}z_{Td} = 3.6$ and in this case $\mu z_{Td} = 1.8$. It also follows from this figure that the interference between the two branches does not violate the Talbot effect.

Let us turn to the fractional dynamical diffraction Talbot effect at depth $z_{Td}/4 = 310\ \mu m$. For comparison, Fig. 3(*a*) shows the intensity distribution in free space for the same wavelength and object at the distance $z_T/4 = 11.3$ m. Here one can see the interference of the initial distribution and the same distribution shifted by $D/2$ and multiplied by the corresponding phases. Fig. 3(*b*) shows the intensity distribution, calculated by the exact formula (5) and by the approximate formula (46) at the depth $z_{Td}/4$, inside the crystal. One can see good agreement of the approximate distribution with the exact one. It can be seen that the intensity distribution in free space has a period two times shorter than inside the crystal. Inside the crystal, the period coincides with the period of the object. To identify the cause, Fig. 3(*b*) shows the intensity distribution inside the crystal for weakly and strongly absorbing branches separately, at the same depth $z_{Td}/4$, calculated using the exact formula (5). It is clear from this figure that the intensity behaviour of both branches is almost the same as in free space, but some modulation is observed, which is apparently due to different absorption of harmonics and from a different dependence of harmonics on the diffraction reflection coefficient inside the crystal. However, because of the interference of both branches, the maxima at $D/2$ are suppressed. The interference of the branches is
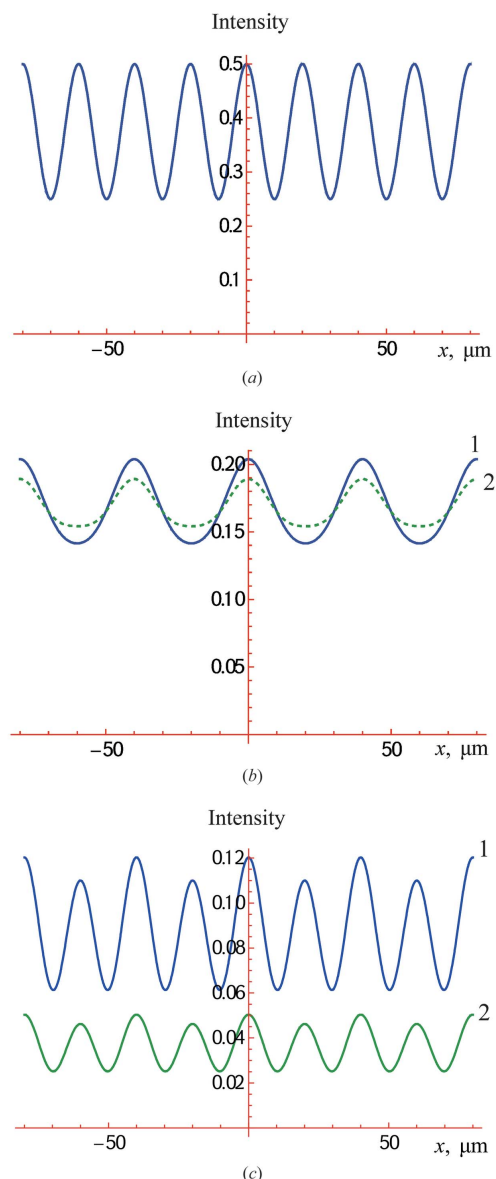

Figure 3
Fractional dynamical diffraction Talbot effect for a cosine-like grating. (*a*) The intensity distribution in free space at the distance $z_T/4$. (*b*) The intensity distribution inside the crystal at the depth $z_{Td}/4$ calculated by the exact formula (5) (curve 1, blue) and by the approximate formula (46) (curve 2, green). (*c*) The intensities of the weakly absorbing (curve 1, blue) and strongly absorbing modes (curve 2, green) calculated by the exact formula (5) at the depth $z_{Td}/4$.

significant, since at the depth $z_{Td}/4$ we have $\mu_{d0+}z_{Td} = 0.02$ and $\mu_{d0-}z_{Td} = 0.9$, and their amplitudes are comparable.

5.2. Ronchi grating

The Ronchi grating (Berry & Klein, 1996) is a system of periodically located slits with a period D and with a slit width $D/2$ [see the inset of Fig. 4(*a*)]. The transmission coefficient $T(x)$ for the Ronchi grating in the unit cell $|x| < D/2$ is given by the expressions $T(x) = 1$ if $|x| < D/4$ and $T(x) = 0$ if $|x| > D/4$. It is supposed that the point with the coordinate $x = 0$ is the centre of one of the slits. For the Ronchi grating, it is easy to
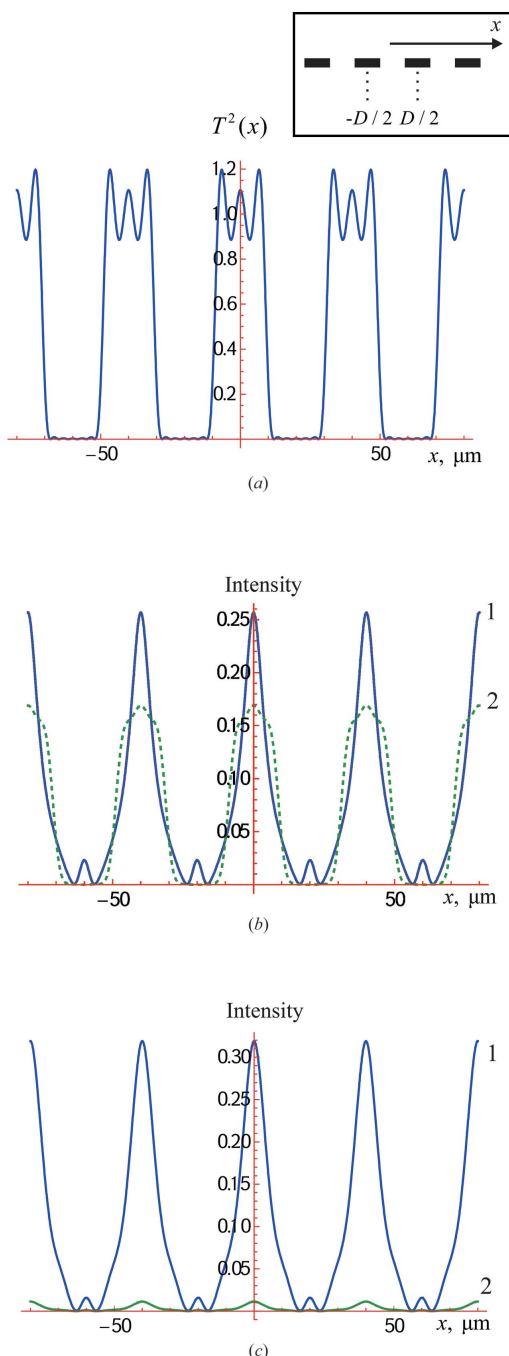
(a)

(b)

(c)

Figure 4
The integral dynamical diffraction Talbot effect at the depth z_{Td} for the Ronchi grating. (*a*) The intensity of the initial distribution $T^2(x)$ (terms up to $|n| = 5$ in Fourier series are left). (*b*) The intensity inside the crystal, according to the exact formula (5) (curve 1, blue) and according to the approximate formula (36) (curve 2, green). (*c*) Comparison of the intensities of the weakly absorbing (curve 1, blue) and strongly absorbing modes (curve 2, green), calculated by the exact formula (5).

see that $A_0 = 0.5$, $A_{2m} = 0$, $A_{2m+1} = (-1)^m/[\pi(2m + 1)]$, $m = 0, \pm1, \pm2, \ldots$. For the period $D = 40$ µm, the condition of the paraxial approximation (23) can be considered as fulfilled up to $|n| = 5$ ($m = -3, -2, \ldots, 2$) inclusively. We will keep in the Fourier series the terms up to $|n| = 5$. In Fig. 4(*a*), the initial distribution $T^2(x)$ is compared with the intensity inside the

crystal, calculated using the exact formula (5) and the approximate formula (36), at the depth z_{Td}. One can see a good agreement of approximate calculations with the exact and initial distribution. To reveal the influence of the interference of the two branches on the Talbot effect, in Fig. 4(*b*) the intensities of strongly and weakly absorbed modes are compared with the total intensity, calculated using the exact formula (5). Fig. 5(*a*) shows the intensity distribution in free space at the distance $z_{\mathrm{T}}/4$. Fig. 5(*b*) shows the intensity distributions at the depth $z_{\mathrm{Td}}/4$, calculated by the exact formula (5) and the approximate formula (46). Fig. 5(*c*) shows the intensity distributions of weakly and strongly absorbed modes at the depth $z_{\mathrm{Td}}/4$, calculated by the exact formula (5).
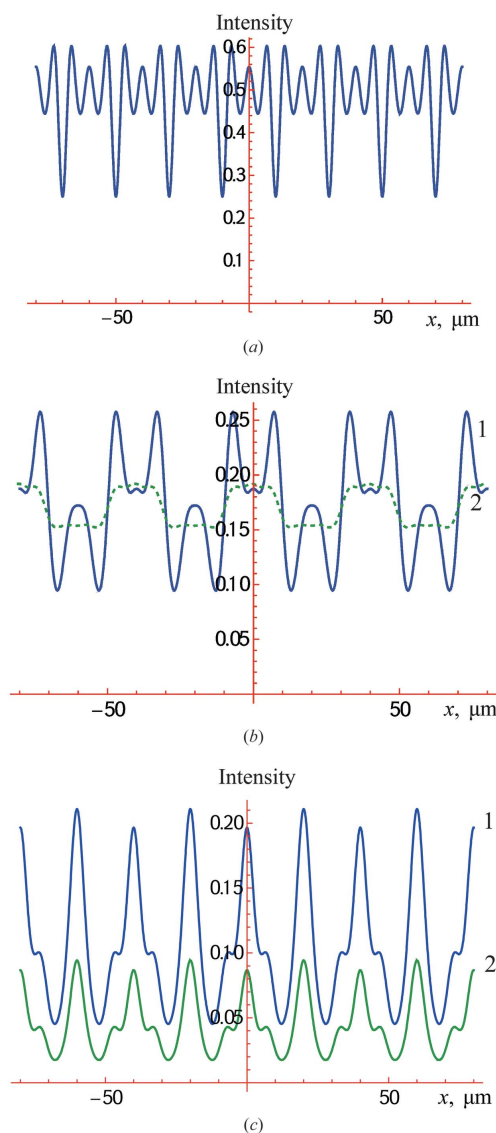

(a)

(b)

(c)

Figure 5
Fractional dynamical diffraction Talbot effect for the Ronchi grating. (*a*) The intensity distribution in free space at the distance $z_{\mathrm{T}}/4$. (*b*) The intensity distribution inside the crystal at the depth $z_{\mathrm{Td}}/4$ calculated by the exact formula (5) (curve 1, blue) and by the approximate formula (46) (curve 2, green). (*c*) The intensities of the weakly absorbing (curve 1, blue) and strongly absorbing modes (curve 2, green) calculated by the exact formula (5) at the depth $z_{\mathrm{Td}}/4$.
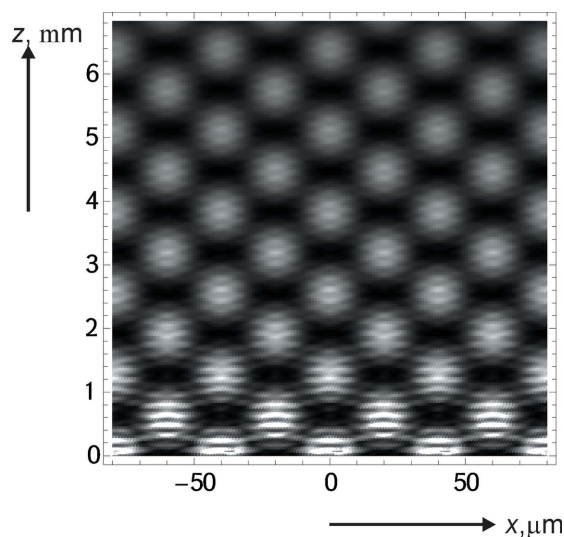
Figure 6
Dynamical diffraction Talbot carpet for the Ronchi grating inside the crystal.

describes well the Talbot effect inside the crystal. The dynamical diffraction Talbot distance is polarization sensitive. At the rational multiple depths of the Talbot depth the wavefield amplitude for each dispersion branch is a coherent sum of the initial distributions, shifted by rational multiple of the object period and having its own phases. The dynamical diffraction Talbot image for a phase object, different from the Talbot image in free space, at integer multiples of Talbot distance, has an inhomogeneous intensity distribution due to absorption and deviation parameter dependence of the spatial harmonics of the initial distribution, inside the crystal.

Dynamical diffraction Talbot carpets and Pendellösung fringes inside the crystal can be observed by means of a wedge-shaped crystal.

Possible applications of the dynamical diffraction Talbot effect can be investigations of crystal structure, investigations of periodic and non-periodic objects, using X-rays, electron and neutron waves and so on.

Finally, Fig. 6 shows the intensity distribution inside the crystal up to the depth $5.5z_{Td}$ (dynamical diffraction Talbot carpet). It is seen that the spots of the initial distribution are accompanied by Pendellösung fringes. At large depths, the Pendellösung fringes lose their contrast due to the absorption of the strongly absorbing mode.

Note that the Talbot carpet inside the crystal can be observed using the same technique, as in the case of Pendellösung fringes (Pinsker, 1982), *i.e.* using a wedge-shaped crystal, with the top line, being perpendicular to the reflecting atomic planes (Balyan, 2019).

6. Summary

In this article the integer and fractional Talbot effect is studied under two-wave dynamical diffraction conditions in a perfect crystal, for the symmetrical Laue case of diffraction. The fractional dynamical diffraction Talbot effect is studied for the first time.

The well known dynamical diffraction effects without a periodic object, *i.e.* extinction modulations (Pendellösung fringes), the Borrman effect, polarization sensitivity of Bragg diffraction and sensitivity of the diffracted wave intensity to the deviation of the incident wave from the Bragg exact direction, accompanies the Talbot effect inside the crystal.

The dynamical diffraction comb wave for the diffracted wave, corresponding to the incidence Dirac comb wave,

References

Authier, A. (2001). *Dynamical Theory of X-ray Diffraction.* Oxford University Press.
Balyan, M. K. (2019). *J. Opt.* **21**, 055603.
Berry, M. V. & Bodenschatz, E. (1999). *J. Mod. Opt.* **46**, 349–365.
Berry, M. V. & Klein, S. (1996). *J. Mod. Opt.* **43**, 2139–2164.
Case, W. B., Tomandl, M., Deachapunya, S. & Arndt, M. (2009). *Opt. Express*, **17**, 20966–20974.
Cloetens, P., Guigay, J. P., De Martino, S., Baruchel, J. & Schlenker, M. (1997). *Opt. Lett.* **22**, 1059–1061.
Dennis, M. R., Zheludev, N. I. & García de Abajo, F. J. (2007). *Opt. Express*, **15**, 9692–9700.
Edgar, R. F. (1969). *Opt. Acta: Int. J. Opt.* **16**, 281–287.
Guigay, G. P. (1971). *Opt. Acta: Int. J. Opt.* **18**, 677–682.
Kim, J. M., Cho, I. H., Lee, S. Y., Kang, H. C., Conley, R., Liu, Ch., Macrander, A. T., Noh, D. Y. & do, Y. (2010). *Opt. Express*, **18**, 24975–24982.
Kim, M.-S., Scharf, T., Menzel, C., Rockstuhl, C. & Herzig, H. P. (2013). *Opt. Express*, **21**, 1287–1300.
Kohn, V. G. (2016). *J. Synch. Investig.* **10**, 698–704.
Kohn, V. G. (2018). *J. Synchrotron Rad.* **25**, 425–431.
Momose, A., Kawamoto, S., Koyama, I., Hamaishi, Y., Takai, K. & Suzuki, Y. (2003). *Jpn. J. Appl. Phys.* **42**, L866–L868.
Momose, A., Yashiro, W., Maikusa, H. & Takeda, Y. (2009). *Opt. Express*, **17**, 12540–12545.
Pinsker, Z. G. (1982). *X-ray Crystalloptics.* Moscow: Nauka. (In Russian.)
Rayleigh, L. (1881). *London, Edinb. Dubl. Philos. Mag. J. Sci.* **11**, 196–205.
Takagi, S. (1962). *Acta Cryst.* **15**, 1311–1312.
Takagi, S. (1969). *J. Phys. Soc. Jpn*, **26**, 1239–1253.
Talbot, H. F. (1836). *Philos. Mag.* **9**, 401–407.